DOI: 10.1002/ejic.201001155

Synthesis and Theoretical Hirshfeld Analysis of a Supramolecular Heteropolyoxovanadate Architecture

Mathias Grabau,[a] Johannes Forster,[a] Kirsten Heussner,[a] and Carsten Streb*[a]

Keywords: Vanadium / Polyoxometalates / Supramolecular chemistry / Hirshfeld surface analysis / Self-assembly / Crystal engineering

A supramolecular heteropolyoxovanadate structure has been synthesized and characterized using single-crystal XRD, powder XRD and a range of spectroscopic methods. The new compound, $[t\text{BuNH}(C_2H_4OH)_2]_4[H_5P_1V_{14}O_{42}]\cdot 12H_2O$ (**1**) was obtained using a one-pot strategy starting from a simple inorganic vanadium oxide precursor and an amphiphilic cation in acidic aqueous solution. The cluster anion $[H_5P_1V_{14}O_{42}]^{4-}$ is based on the well-known Keggin structure but in addition features two capping vanadyl $[V{=}O]^{3+}$ units. In the crystal lattice, the clusters are arranged in linear 1D chains where neighbouring clusters are directly linked by one hydrogen bond. In addition, the assembly is stabilized by lattice water molecules and organic counterions which aggregate to form hydrophobic cavities with diameters of 0.6 nm. In order to analyze the supramolecular interactions leading to the cluster formation, we have used a combination of traditional structural analysis, theoretical bond valence sum (BVS) calculations and computational Hirshfeld surface analyses which allow the rapid determination of short- and long-range intermolecular contacts. The applicability of the Hirshfeld analysis tool for complex ionic compounds is evaluated and the advantages as well as the limitations of the method are discussed. The combination of these techniques allowed us to assess the dominating intermolecular interactions and showed that the crystal packing is not only controlled by electrostatic interactions, but also by distinctive sets of hydrogen bonds and hydrophobic interactions between adjacent organic counterions.

Introduction

The self-assembly of complex systems starting from simple building blocks has fascinated scientists from various fields of research for many centuries.[1] The resulting structures not only increase in size and complexity, but often feature novel, unexpected synergistic properties which are established due to the combined interaction of the assembled building blocks.[2] One key concept that employs exactly this self-assembly mechanism is the formation of organic–inorganic materials where the properties of both organic and inorganic building units contribute to the resulting material properties.[3] In particular the self-assembly of molecular metal oxide clusters[4–6] in the presence of organic counterions has sparked a wide range of research activities in areas as diverse as electronics,[7] magnetism,[8] catalysis[9] through to nanomaterials[10] and biological-medical applications.[11] This is due to the fact that these metal oxide clusters, or polyoxometalates, are highly versatile building units which can adopt a wide range of structures ranging from six up to 368 metal centres[6] and can incorporate a wide selection of chemical elements which allow the fine-tuning of the desired cluster properties.[4]

Inspired by these complex supramolecular architectures, we have set out to investigate the in-situ self-assembly of vanadium oxide clusters[12] in the presence of amphiphilic organic cations. This concept was thought to allow us the assembly of a supramolecular structure where the organocation can establish hydrophobic intermolecular interactions with other counterions and also form strong hydrophilic interactions with the cluster surface via the hydrophilic moieties. This was thought to provide an ideal example of a complex self-assembled material which would allow us to study the intricate cooperative effects of the combined interaction of a wide range of supramolecular forces. In addition to standard structural investigation, we planned to conduct a computational Hirshfeld analysis[13] of the material which allows a more general evaluation of the effects of the intermolecular interactions observed.

Results and Discussion

The synthetic approach employed in this study is a classic one-pot strategy that is often used in the synthesis of metal oxide cluster systems.[14] We opted to assemble a polyoxovanadate unit around a central phosphate template[14] by acidifying an aqueous vanadate solution with dilute phos-

[a] Department of Chemistry and Pharmacy, Institute of Inorganic Chemistry II, Friedrich-Alexander-University Erlangen-Nuremberg,
Egerlandstr. 1, 91058 Erlangen, Germany
Fax: +49-9131-27367
E-mail: carsten.streb@chemie.uni-erlangen.de
www.strebgroup.net

Supporting information for this article is available on the WWW under http://dx.doi.org/10.1002/ejic.201001155.

phoric acid. In order to obtain an organic–inorganic structure for the detailed study of a range of supramolecular interactions, we decided to introduce an amphiphilic counterion, *tert*-butyldiethanolamine, tBuN($C_2H_4OH)_2$ which under the given reaction conditions is protonated to the corresponding ammonium cation. In order to avoid the formation of purely inorganic crystalline materials, the organocation was employed in fivefold excess. This synthetic approach allowed us to isolate compound **1** within 24 h crystallization time in yields of more than 90% (based on V).

Single-crystal X-ray diffraction analysis showed that compound **1** crystallizes in the highly symmetric tetragonal space group *I*-4 with axis lengths of $a = b = 16.9573$ Å, $c = 13.7367$ Å, $\alpha = \beta = \gamma = 90°$ and gave the unit formula $[t\text{BuNH}(C_2H_4OH)_2]_4[H_5P_1V_{14}O_{42}]\cdot 12H_2O$. Structural analysis of the diffraction data showed that the main inorganic building unit in **1** is a heteropolyoxovanadate cluster, $[H_5P_1V_{14}O_{42}]^{4-}$ (hereafter: $\{P_1V_{14}\}$).[15] The cluster architecture is based on the well-known heteropolyoxometalate archetype, the so-called Keggin cluster $[X_1M_{12}O_{40}]^{n-}$ (X = Si, Ge, P, etc., M = Mo, W).[5] However, for stability reasons, the $\{P_1V_{14}\}$ unit features two additional vanadium centres, taking the overall number of metal centres to 14 per cluster unit. The reason for not forming the original dodecanuclear Keggin unit is due to the accessible oxidation states of vanadium as compared with molybdenum or tungsten: The Keggin architecture is only known for the molybdenum- and tungsten-based systems where the high oxidation states of the metal centres (Mo^{VI}, W^{VI}) allow the efficient stabilization of a relatively low overall cluster charge, resulting in stable molecular cluster units such as $[P_1W_{12}O_{40}]^{3-}$.[5] However, since the highest oxidation state of vanadium is V^V it is obvious that the identical, hypothetical unit $[P_1V_{12}O_{40}]^{15-}$ would have to compensate 15 negative charges resulting in a dramatically increased electrostatic repulsion and thus in a much lower overall stability.

However, from our analysis it is obvious that the vanadium system still attempts to assemble into Keggin units and compensates for the high electrostatic charge by two mechanisms. The main structural compensation proceeds via the incorporation of two vanadyl $[V{=}O]^{3+}$ fragments[16] which are bound to vacant coordination sites formed by four oxo ligands on the cluster shell, thereby reducing the negative cluster charge. Secondary charge compensation is achieved by the fivefold protonation of the cluster shell, resulting in the final cluster formula $[H_5P_1V_{14}O_{42}]^{4-}$, see Scheme 1.

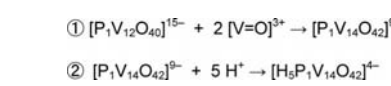

Scheme 1. Charge compensation mechanism resulting in the formation of the Keggin-based $[H_5P_1V_{14}O_{42}]^{4-}$ cluster. Step 1: charge reduction by addition of two $[V{=}O]^{3+}$ vanadyl units. Step 2: fivefold protonation to reduce the cluster charge.

As mentioned earlier, the $\{P_1V_{14}\}$ cluster is structurally closely related to the archetypal Keggin cluster. The centre of the cluster is occupied by a tetrahedral template, in this case a phosphate PO_4^{3-} anion. Each oxygen atom of the phosphate anion acts as the central anchoring site for a so-called $[V_3O_{13}]$ triad where three vanadium(V) centres are linked into a trigonal, C_{3v}-symmetric building unit; each V-centre is linked to the neighbouring groups by one μ_2-bridging oxo ligand with V–O distances of d_{V-O} ca. 1.8–2.0 Å. In addition, each V-centre features one terminal oxo ligand with characteristically short V–O distances of $d_{V-O} = 1.6$ Å, see Figure 1. It is worth noting that the 12 vanadium centres which form the Keggin-based cluster shell form six-coordinate $[VO_6]$ octahedra, whereas the additional vanadyl moieties adopt a square-pyramidal $[VO_5]$ coordination mode.

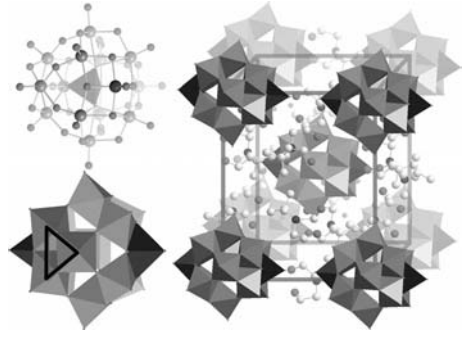

Figure 1. Illustration of the $\{P_1V_{14}\}$ cluster unit and arrangement of the $\{P_1V_{14}\}$ units in the crystal lattice. Left: ball-and-stick representation (top) of the $[H_5P_1V_{14}O_{42}]^{4-}$ heteropolyoxovanadate unit showing the templating phosphate anion as a grey tetrahedron. Polyhedral representation (bottom) of the cluster unit, highlighting the 12 $[VO_6]$ octahedra (light grey polyhedra) and two vanadyl-based $[VO_5]$ square pyramids (dark grey polyhedra). The $[V_3O_{13}]$ triads which are the main building units of the cluster are highlighted by a black triangle. Right: packing diagram of compound **1**, highlighting the *I*-centred arrangement of the clusters within the crystal lattice. Colour scheme C: light grey, N: black, O: dark grey, V: large grey spheres. Hydrogen atoms and lattice water molecules are omitted for clarity.

Theoretical analysis of the cluster structure using bond valence sum (BVS) calculations together with UV/Vis spectroscopy confirms that all vanadium centres are fully oxidized V^V units. In addition, the BVS calculations allowed us to locate the five protonation sites and careful analysis of the metal–oxygen bond lengths based on the single-crystal XRD analysis verified these findings (see below). One main feature of the resulting crystal packing is the *I*-centred arrangement of the $\{P_1V_{14}\}$ cluster units within the crystal lattice, see Figure 1. The analysis of the crystal structure of **1** using a combination of Hirshfeld analysis, traditional manual structural analysis and BVS calculations allowed us to identify a range of highly directed intermolecular interactions which are considered to contribute strongly to the packing of the units in the crystal lattice of compound **1**.

Using a combination of structural analysis and theoretical BVS calculations, we were able to identify five protonation sites on the $\{P_1V_{14}\}$ cluster. The most striking hydro-

gen-bonding feature in compound **1** is the formation of hydrogen-bonded 1D chains of $\{P_1V_{14}\}$ clusters which propagate along the crystallographic *c* axis. Here, the clusters are aligned so that their main molecular axis defined by the two apical vanadyl V=O units lies on the crystallographic *c* axis. Between two adjacent $\{P_1V_{14}\}$ clusters, a single hydrogen bond is formed, resulting in short O···O contacts ($d_{O\cdots O}$ = 2.890 Å). Interestingly, this protonation is located on the oxygen ligand O5 which is part of the apical vanadyl unit, highlighting the importance of these additional vanadium centres for the supramolecular architecture. This hydrogen-bonding pattern is repeated on the opposite side of the cluster, resulting in the formation of a linear 1D cluster chain.

The second cluster protonation site is located on O1 and was determined by combined structural analysis and BVS analysis. Because of the fourfold cluster symmetry, the single protonation on O1 results in four protonation sites when the crystallographic symmetry elements are applied so that the complete cluster is fivefold protonated, which is in line with our crystallographic sum formula determination and the elemental analysis. Because of the I-centred cluster packing in the crystal lattice, an ABAB-type layering can be observed so that one hydrogen-bonded chain is located in the centre of the unit cell and four chains are located on the unit cell edges, all aligned in a co-parallel fashion along the crystallographic *c* axis, see Figure 2. The minimum distance between adjacent chains is ca. 5.2 Å, observed between offset chains located in the centre and on the edge of a unit cell, respectively, so that any intermolecular interactions between chains can be excluded.

The separation of 1D chains in the crystal lattice of **1** is achieved by the presence of the *tert*-butyldiethanolammonium (hereafter: BDA) cations which act as supramolecular spacers between neighbouring sets of cluster chains. It is intriguing to note that these counterions are arranged in a fashion so as to form hydrophobic cavities. These structures are formed by the aggregation of the bulky, hydrophobic *tert*-butyl substituents on the BDA cations so that four of these substituents enclose a central cavity. The hydrophilic hydroxyethyl substituents point away from this cavity towards the hydrophilic $\{P_1V_{14}\}$ units, resulting in the formation of hydrogen bonds between the hydroxyethyl moiety and the oxo ligands on the cluster. As a result, a 2D arrangement of hydrophobic cavities is formed; each cavity enclosing a central void with a diameter of about 0.63 nm, see Figure 2.

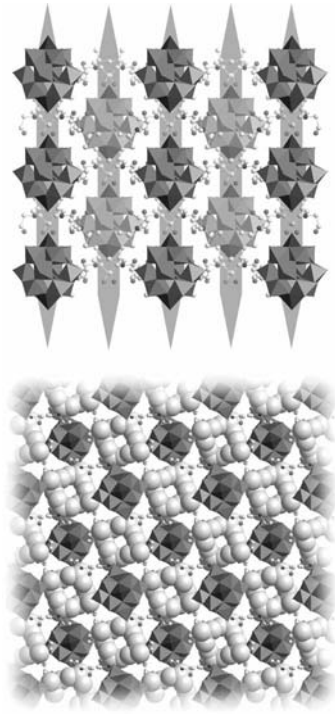

Figure 2. Illustration of the supramolecular aggregation observed in compound **1**. Top: crystal packing along the crystallographic *a* axis, showing the formation of hydrogen-bonded 1D chains of $\{P_1V_{14}\}$ clusters (highlighted by grey arrows). Hydrogen bonds are formed between adjacent vanadyl V=O oxo ligands on opposite sides of the cluster shell. Bottom: formation of hydrophobic cavities (d = 0.63 nm) formed by aggregation of four *tert*-butyl substituents on four adjacent BDA counterions.

Recently, a new method has been introduced by McKinnon and Spackman[13] which allows the qualitative and quantitative investigation and visualization of intermolecular close contacts within a supramolecular crystal lattice. This so-called Hirshfeld analysis[17] can be employed to calculate isosurfaces for molecular fragments within a crystal lattice which can be interpreted as boundaries between separated molecular structures within the lattice. These theoretical calculations are conducted using spherically averaged Hartree–Fock electron density functionals[18] based on the nuclei in question. As a result, an isosurface is obtained on which a range of parametrical functions (such as distance to the next atom inside/outside the Hirshfeld surface, surface curvature, etc.) can be plotted and visualized. The advantage of this method is that it gives an immediate and general overview of the molecular sites where short- and long-range intermolecular contacts (i.e. strong and weak intermolecular interactions) are observed. The separation into distinct sets of intermolecular distances (e.g., H···H, O···H, etc.) therefore allows the facile assignment to a certain type of interaction; for example, a short O···H contact is characteristic for an intermolecular hydrogen bond. Using this analysis, one has to bear in mind the limitations of the underlying approach: (I) the method requires high-quality single-crystal XRD data with atomic resolution and correct assignment of the atomic species, as all analysis carried out relies on crystallographically well-defined interatomic distances within the structure; (II) to analyze the interactions between two molecules, the hydrogen atom positions on these molecules need to be determined crystallographically or computationally to allow the exact determination of hydrogen-related interactions. This is particularly problematic if the interactions with water molecules within the crystal lattice are to be investigated, as the determination of the hydrogen atoms on the water molecule is not trivial; (III) the method does not identify purely electrostatic (Coulomb) interactions as these are not

directly reflected in the intermolecular distances of the crystal structure.

Bearing in mind these limitations, it is obvious that the Hirshfeld analysis cannot provide detailed insight into the purely electrostatic aggregation of cations and anions or for example, the role of water molecules in large hydrogen-bonded networks. For these reasons, Hirshfeld analyses have been mostly employed for purely organic, non-charged systems.[13] However, if the structural analysis is focussed on the supramolecular interactions and the above criteria are met, the approach can be used to investigate the interactions which determine the supramolecular architecture of a given crystal lattice. In this instance, we were interested in the effects of hydrophobic and hydrogen-bonding interactions in the case of compound **1**.

In addition, the Hirshfeld analysis allows the determination of 2D fingerprint plots in which the distance from the Hirshfeld surface to an internal nucleus (d_i) is plotted against the distance of the Hirshfeld surface to an external nucleus (d_e). These plots can be determined for pairs of nuclei inside and outside the Hirshfeld surface (e.g., O inside, H outside, representing an incoming hydrogen bond) and a quantitative assignment can be made as to how big the percentage contribution of this type of close contacts is for the molecule under investigation.[13] *Note:* This analysis requires the full structural characterization (including all hydrogen atoms) of the molecules in question.

In this example, the Hirshfeld approach is used for the first time in the analysis of a polyoxometalate-based system. We chose to conduct this investigation to demonstrate the feasibility of this approach and to evaluate the information obtained as well as to determine the limitations of the technique. In addition, we were interested in implementing a new technique which gives an instant overview of the supramolecular interactions observed. Such a technique would be an advantage as traditionally, polyoxometalate-based systems are mainly characterized in terms of the electrostatic (cation–anion) and hydrogen-bonding interactions as the complete manual evaluation of intermolecular contacts, in particular when complex organic cations are involved, requires a vast amount of time and is therefore often neglected. Important information on weak interactions can therefore be missed.

Hirshfeld analysis of the BDA cation in **1** shows two distinct regions within the molecule: for the hemisphere around the *tert*-butyl substituent, few close contacts are observed, indicating the absence of strong intermolecular interactions. This is in line with the presence of long-range hydrophobic interactions, leading to the formation of the hydrophobic cavities in **1**. However, in the region around the protonated amine and the hydroxy groups, a multitude of close intermolecular contacts are observed which correspond to a range of incoming and outgoing hydrogen bonds where the BDA cation interacts with the $\{P_1V_{14}\}$ cluster surface and with lattice water molecules, see Figure 3. This also shows a limitation of this analysis, as interactions with hydrogen-bonded water molecules cannot be unequivocally determined. For this, we conducted a manual structural analysis and it was shown that the hydroxyethyl arms of the BDA molecule form four hydrogen bonds to neighbouring lattice water molecules ($d_{O\cdots O}$ = 2.58–2.92 Å).

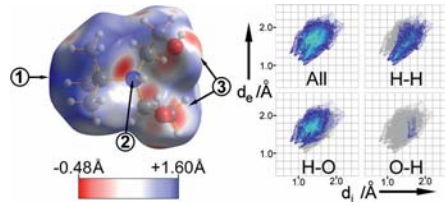

Figure 3. Hirshfeld analysis of the BDA counterion in **1**. Left: Hirshfeld surface, with normalized intermolecular distances d_{norm}[19] plotted onto the surface. *Note*: negative d_{norm} values represent intermolecular distances shorter than the sum of the van der Waals radii, positive d_{norm} values represent distances longer than the sum of the van der Waals radii; (1): hydrophobic long-range H–H interactions; (2): intramolecular hydrogen bond from the ammonium ion to the hydroxyethyl group; (3): hydrogen-bonded hydroxyethyl groups. Colour code: red: short intermolecular contacts, blue: long intermolecular contacts. Right: 2D fingerprint plots[19] for selected contacts plotting the distance of the internal nucleus (d_i) and the distance of the external nucleus (d_e) from the Hirshfeld surface. For instance, H–O shows d_i of the internal nucleus (H) against d_e of the external nucleus (O), thus representing close contacts between hydrogen atoms on the internal BDA molecule with external oxygen atoms.

Analysis of the 2D fingerprint plots allowed the quantitative rationalization of the close contacts observed for the BDA molecule. The main contribution to intermolecular close contacts is based on hydrogen atoms on the BDA molecule, 93.6%, whereas only 6.4% of all contacts are based on the hydroxy oxygen atoms. In addition, 38.5% of the contacts are close H–H contacts, suggesting a considerable contribution of hydrophobic interactions in the formation of the crystal lattice, see Table 1.

Table 1. Quantitative Hirshfeld fingerprint analysis giving percent contribution of specific contacts to the overall sum of intermolecular contacts between the BDA cation and the surrounding molecules.

Nucleus inside Hirshfeld surface	Nucleus outside Hirshfeld surface	Percent contribution
All	All	100
H	All	93.6
H	H	38.5
H	O	55.1
O	All	6.4
O	H	1.1
O	O	5.3

The Hirshfeld analysis for the $\{P_1V_{14}\}$ polyoxovanadate cluster shows that the principal interactions are hydrogen bonds resulting from the protonation of the cluster as well as from the bonding of protonated species (hydroxyethyl groups on the BDA cation and lattice water). In particular it is noteworthy that this visualization approach allowed the instant identification of hydrogen-bonded protonated oxo groups on the cluster (i.e. V–O–H···O) and their discrimination from cluster oxo sites which act as hydrogen-bond acceptors (i.e. V–O···H–O), see Figure 4. This was confirmed by BVS calculations and by manual comparison

with the corresponding hydrogen-bonded short contacts ($d_{O\cdots O}$ = 2.61–2.94 Å) observed in the single-crystal dataset of **1**.

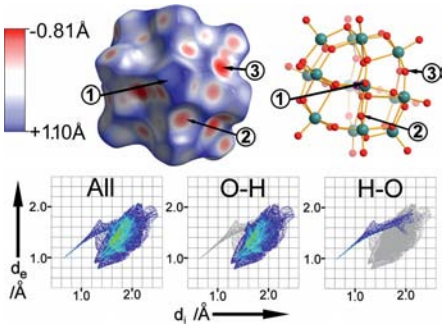

Figure 4. Hirshfeld analysis of the $\{P_1V_{14}\}$ cluster in **1**. Top: Hirshfeld surface (left), with normalized intermolecular distances d_{norm}[19] plotted onto the surface. Right: ball-and-stick representation of $\{P_1V_{14}\}$. A non-hydrogen-bonded terminal oxo group (1), an incoming hydrogen bond to a μ_2-bridging cluster oxo ligand (2) and an outgoing hydrogen bond from a cluster μ_2-OH hydroxy group (3) can be identified. Colour code: red: short intermolecular contacts, blue: long intermolecular contacts. Bottom: 2D fingerprint plots[19] for selected contacts plotting the distance of the internal nucleus (d_i) and the distance of the external nucleus (d_e) from the Hirshfeld surface.

As expected from structural considerations, analysis of the 2D fingerprint plots of $\{P_1V_{14}\}$ showed that the main contribution of intermolecular contacts is formed between cluster oxo groups and external hydrogen atoms, i.e. hydroxyethyl groups on the BDA molecule (contribution: 73.7%). In addition, it was shown that cluster proton-based interactions contribute 10.5% to the overall intermolecular interactions of the cluster, thus suggesting a considerable stabilization of the cluster in the supramolecular lattice through hydrogen-bonding interactions, see Table 2.

Table 2. Quantitative Hirshfeld 2D fingerprint analysis giving percent contribution of specific contacts to the overall sum of intermolecular contacts between the cluster anion $\{P_1V_{14}\}$ and the surrounding molecules.

Nucleus inside Hirshfeld surface	Nucleus outside Hirshfeld surface	Percent contribution
All	All	100
O	All	89.5
O	H	73.7
O	O	15.8
H	All	10.5
H	O	7.0
H	H	3.5

Conclusions

In conclusion, we have shown that weak, hydrophobic interactions in an ionic system can lead to the formation of supramolecular spatial separation and the formation of small, hydrophobic cavities in the crystal lattice. We have employed a combination of structural analysis, theoretical BVS calculations and computational Hirshfeld analysis to rationalize the intermolecular interactions within this supramolecular system. The usefulness of Hirshfeld analysis in complex systems has been critically evaluated and it was shown that if the limiting criteria are observed, Hirshfeld analysis can be a valuable tool that speeds up the structural analysis and is particularly useful to qualitatively and quantitatively assess the interactions observed around a molecule. However, from this study it is also obvious that the method is limited by the necessity of high-quality crystallographic data and the determination of all hydrogen atoms in the structure. In addition, the results require further investigation using additional techniques such as manual interatomic distance analyses and theoretical BVS calculations to provide meaningful results. Of particular interest is the identification of weak, long-range intermolecular contacts which are often neglected in complex systems. In summary, the Hirshfeld analysis can play an important role in the rapid analysis of complex molecular architectures and the results can be used as a basis for more detailed structural analyses.

Experimental Section

Materials and Methods: All chemicals were purchased from Sigma Aldrich and Acros (reagent grade) and were used as received. FT-IR spectra (KBr pellets) were recorded with a Shimadzu FT-IR-8400S FT-IR spectrometer. Elemental analyses were performed with a Euro Vector Euro EA 3000 elemental analyzer. UV/Vis spectra were recorded with a Varian Cary 50 UV/Vis spectrophotometer or a Shimadzu PharmaSpec 1700 UV/Vis spectrophotometer. Powder XRD analysis was performed with a Philips X'PERT 1 powder diffractometer.

$[t$BuNH$(C_2H_4OH)_2]_4[H_5P_1V_{14}O_{42}]\cdot 12H_2O$ (1): V_2O_5 (1.0 g, 5.5 mmol) was dissolved in aqueous NaOH solution (5 M, 40 mL). To this, tBuN$(C_2H_4OH)_2$ (1.34 g, 1.5 equiv., 8.3 mmol) was added under vigorous stirring. The solution pH was adjusted to pH = 3.0 using H_3PO_4 (2 M). Upon acidification, the colour of the solution changed from colourless to deep red. The reaction mixture was covered and kept at room temperature for 24 h to give deep red crystals of **1**; yield 1.69 g (0.74 mmol, 94.2% based on V). Elemental analysis for dehydrated **1**, $C_{32}H_{91}N_4O_{53}P_1V_{14}$: calcd. C 18.09, H 4.32, N 2.63; found C 18.15, H 4.56, N 2.46. IR (KBr): $\tilde{\nu}$ = 3320 (b), 1628 (w), 1475 (w), 1383 (m), 1269 (w), 1182 (w), 1071 (m), 1047 (m), 950 (s), 878 (m), 804 (m), 735 (m), 594 (m) cm^{-1}. ^1H NMR (269.71 MHz, D_2O): δ = 1.26 (s), 3.04 (t), 3.1 (t), 3.14 (s), 3.4–3.55 (m/qu), 3.78 (t), 4.63 (s) ppm. UV/Vis: $\lambda_{max,1}$ = 441 nm (ε = 3.25×10^3 $M^{-1}cm^{-1}$), $\lambda_{max,2}$ = 229 nm (ε = 1.15×10^4 $M^{-1}cm^{-1}$). Powder X-ray diffractometry peaks observed (expected from single-crystal data) in degrees 2Θ: 7.46 (7.37), 8.29 (8.28), 20.60 (21.0), 21.01 (21.09), 30.71 (30.98).

Single-Crystal X-ray Crystallography: Suitable single crystals of **1** were grown and mounted onto the end of a thin glass fibre. X-ray diffraction intensity data were measured at 150 K with a Nonius Kappa CCD diffractometer [λ(Mo-K_α) = 0.71073 Å] equipped with a graphite monochromator. Structure solution and refinement was carried out using the SHELX-97 package[20] via WinGX.[21] Corrections for incident and diffracted beam absorption effects were applied using empirical[22] or numerical methods.[23] Structures were solved by a combination of direct methods and difference Fourier syntheses and refined against F^2 by the full-matrix least-squares technique. Crystal data, data collection parameters and re-

finement statistics for **1**: $[t\text{BuNH}(C_2H_4OH)_2]_4[H_5P_1V_{14}O_{42}]\cdot 12H_2O$, Mw = 2257.12 g mol^{-1}, tetragonal, space group I-4, $a = b$ = 16.9573(11) Å, c = 13.7367(9) Å, V = 3950.0(6) Å^3, Z = 2, μ(Mo-K_α) = 1.707 cm^{-1}, 37459 reflections collected, 2111 unique which were used in all calculations; final R_1 = 0.0252 and wR_2 = 0.0670 (all data).

CCDC-798324 (for **1**) contains the supplementary crystallographic data for this paper. These data can be obtained free of charge from The Cambridge Crystallographic Data Centre via www.ccdc.cam.ac.uk/data_request/cif.

Hirshfeld Analysis: Hirshfeld analysis and generation of 2D fingerprint plots was carried out using the program *CrystalExplorer* (v2.1) by K. Wolff, D. J. Grimwood, J. J. McKinnon, M. J. Turner, D. Jayatilaka, M. A. Spackman, University of Western Australia, 2010.[13] Hirshfeld surfaces were generated based on all molecular fragments within a radius of 5.0 Å around a given molecule.

Supporting Information (see footnote on the first page of this article): The full computational Hirshfeld analysis is available.

Acknowledgments

The authors gratefully acknowledge the support of The Institute of Inorganic Chemistry II (FAU). The Fonds der Chemischen Industrie (FCI) is gratefully acknowledged for providing a Liebig Fellowship (to C. S.) and a doctoral fellowship (to J. F.).

[1] a) V. Balzani, M. Gomez-Lopez, J. F. Stoddart, *Acc. Chem. Res.* **1998**, *31*, 405; b) J. F. Stoddart, *Chem. Soc. Rev.* **2009**, *38*, 1802; c) G. M. Whitesides, M. Boncheva, *Proc. Natl. Acad. Sci. USA* **2002**, *99*, 4769.
[2] A. Müller, S. Roy, *Coord. Chem. Rev.* **2003**, *245*, 153.
[3] a) P. J. Hagrman, D. Hagrman, J. Zubieta, *Angew. Chem. Int. Ed.* **1999**, *38*, 2639; b) A. P. Wight, M. E. Davis, *Chem. Rev.* **2002**, *102*, 3589; c) V. Shivaiah, M. Nagaraju, S. K. Das, *Inorg. Chem.* **2003**, *42*, 6604.
[4] a) D. L. Long, E. Burkholder, L. Cronin, *Chem. Soc. Rev.* **2007**, *36*, 105; b) D. L. Long, R. Tsunashima, L. Cronin, *Angew. Chem. Int. Ed.* **2010**, *49*, 1736.
[5] M. T. Pope, *Heteropoly and Isopoly Oxometalates*, Springer, Heidelberg, **1983**.
[6] M. T. Pope, A. Müller, *Angew. Chem. Int. Ed. Engl.* **1991**, *30*, 34.
[7] a) E. Coronado, C. J. Gomez-Garcia, *Chem. Rev.* **1998**, *98*, 273; b) J. M. Poblet, X. Lopez, C. Bo, *Chem. Soc. Rev.* **2003**, *32*, 297.
[8] a) E. Coronado, J. R. Galan-Mascaros, C. Gimenez-Saiz, C. J. Gomez-Garcia, S. Triki, *J. Am. Chem. Soc.* **1998**, *120*, 4671; b) U. Kortz, A. Müller, J. van Slageren, J. Schnack, N. S. Dalal, M. Dressel, *Coord. Chem. Rev.* **2009**, *253*, 2315; c) C. Ritchie, A. Ferguson, H. Nojiri, H. N. Miras, Y. F. Song, D. L. Long, E. Burkholder, M. Murrie, P. Kögerler, E. K. Brechin, L. Cronin, *Angew. Chem. Int. Ed.* **2008**, *47*, 5609.
[9] a) N. S. Antonova, J. J. Carbo, U. Kortz, O. A. Kholdeeva, J. M. Poblet, *J. Am. Chem. Soc.* **2010**, *132*, 7488; b) A. M. Khenkin, G. Leitus, R. Neumann, *J. Am. Chem. Soc.* **2010**, *132*, 11446; c) Y. Kikukawa, K. Yamaguchi, N. Mizuno, *Angew. Chem. Int. Ed.* **2010**, *49*, 6096.
[10] a) A. Nisar, J. Zhuang, X. Wang, *Chem. Mater.* **2009**, *21*, 3745; b) C. Streb, R. Tsunashima, D. A. MacLaren, T. McGlone, T. Akutagawa, T. Nakamura, A. Scandurra, B. Pignataro, N. Gadegaard, L. Cronin, *Angew. Chem. Int. Ed.* **2009**, *48*, 6490.
[11] a) K. Micoine, B. Hasenknopf, S. Thorimbert, E. Lacote, M. Malacria, *Angew. Chem. Int. Ed.* **2009**, *48*, 3466; b) B. Hasenknopf, *Front. Biosci.* **2005**, *10*, 275.
[12] a) A. Müller, M. Penk, R. Rohlfing, E. Krickemeyer, J. Döring, *Angew. Chem. Int. Ed. Engl.* **1990**, *29*, 926; b) W. G. Klemperer, T. A. Marquart, O. M. Yaghi, *Angew. Chem. Int. Ed. Engl.* **1992**, *31*, 49; c) D. Gatteschi, L. Pardi, A.-L. Barra, A. Müller, *Mol. Eng.* **1993**, *3*, 157.
[13] a) J. J. McKinnon, M. A. Spackman, A. S. Mitchell, *Acta Crystallogr., Sect. B* **2004**, *60*, 627; b) M. A. Spackman, D. Jayatilaka, *CrystEngComm* **2009**, *11*, 19; c) M. A. Spackman, J. J. McKinnon, *CrystEngComm* **2002**, *4*, 378.
[14] C. P. Pradeep, D. L. Long, C. Streb, L. Cronin, *J. Am. Chem. Soc.* **2008**, *130*, 14946.
[15] a) M. I. Khan, J. Zubieta, P. Toscano, *Inorg. Chim. Acta* **1992**, *193*, 17; b) S. Nakamura, T. Yamawaki, K. Kusaka, T. Otsuka, T. Ozeki, *J. Cluster Sci.* **2006**, *17*, 245.
[16] M. Piepenbrink, M. U. Triller, N. H. J. Gorman, B. Krebs, *Angew. Chem. Int. Ed.* **2002**, *41*, 2523.
[17] F. L. Hirshfeld, *Theor. Chim. Acta* **1977**, *44*, 129.
[18] a) C. Roetti, E. Clementi, *J. Chem. Phys.* **1974**, *60*, 4725; b) C. Roetti, E. Clementi, *J. Chem. Phys.* **1974**, *60*, 3342; c) E. Clementi, C. Roetti, *At. Data Nucl. Data Tables* **1974**, *14*, 177.
[19] $d_{norm} = [(d_i - r_{i,vdW})/r_{i,vdW}] + [(d_e - r_{e,vdW})/r_{e,vdW}]$ with d_{norm} = normalized contact distance; $d_{i/e}$ = internal/external distance between Hirshfeld surface and nucleus; $r_{i/e,vdW}$ = van der Waals radius of the internal/external nucleus; negative values represent intermolecular distances shorter than the sum of the van der Waals radii, positive values represent distances longer than the sum of the van der Waals radii; see also: J. J. McKinnon, D. Jayatilaka, M. A. Spackman, *Chem. Commun.* **2007**, 3814.
[20] G. M. Sheldrick, *Acta Crystallogr., Sect. A* **2008**, *64*, 112.
[21] L. J. Farrugia, *J. Appl. Crystallogr.* **1999**, *32*, 837.
[22] R. H. Blessing, *Acta Crystallogr., Sect. A* **1995**, *51*, 33.
[23] P. Coppens, L. Leiserowitz, D. Rabinovich, *Acta Crystallogr.* **1965**, *18*, 1035.

Received: October 28, 2010
Published Online: March 1, 2011

